ChemComm

Accepted Manuscript

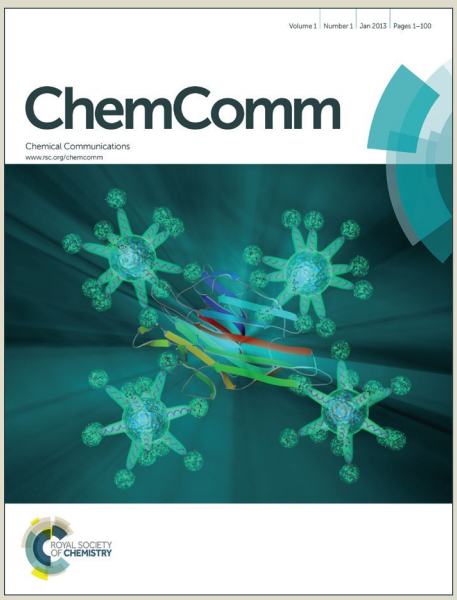

ROYAL SOCIETY OF CHEMISTRY

www.rsc.org/chemcomm

COMMUNICATION

Gold-plated silver nanoparticles engineered for sensitive plasmonic detection amplified by morphological changes†

Received 00th January 20xx,
Accepted 00th January 20xx

DOI: 10.1039/x0xx00000x

www.rsc.org/

Krysten Hobbs, Nicole Cathcart and Vladimir Kitaev[a]

Gold-plated silver nanoparticles have been developed to undergo morphological changes that enhance the surface plasmon resonance (SPR) sensing response. These morphological changes were realized through thin-frame gold plating that both reinforces the nanoparticle edges and enables partial silver etching upon exposure to several biological molecules, including thiols and amines.

Metal nanoparticles (MNPs) established their utility in various applications due to diverse advantageous properties.[1,2] The current thrust in MNP research is to engineer nanoscale morphologies[3,4] with their tailorable properties[5] for specific functional applications.[6,7] Surface enhanced Raman spectroscopy (SERS) and surface plasmon resonance (SPR) spectroscopy are two sensing applications where gold and silver NPs are advantageous.[8,9,10] In particular, SPR spectroscopy with MNPs has become more practical due to its relative simplicity and cost-effectiveness. Compared with conventional SPR based upon thin gold films, MNPs have no angular restriction in light coupling with the localized surface plasmon resonance (LSPR) and LSPR tunability.[11] SPR commonly refers to an analytical technique, while LSPR is a characteristic property of plasmonic MNPs. The SPR signal originates from the refractive index changes at the MNP interface, e.g. caused by chemisorption.[12] Anisotropic and shell MNPs have the potential to provide the best SPR sensitivity,[13,14] while being prone to morphological changes, such as etching or changes in shell dimensions.[15] These changes can either exert a detrimental effect or be utilized for the advantage of SPR-based sensing.

Silver NPs offer superior optoelectronic properties and NP shape control, but are more problematic with chemical stability, limiting their applications in SPR sensing. Gold plating is one of the proven solutions to enhance stability of silver NPs.[6,16] Coating of silver on AuNPs[17,18] is also a noteworthy direction for enhanced SPR sensing.[19,20] The amount of gold attainable with continuous gold plating is limited due to the fast rates of galvanic replacement.[21,22] Despite this limitation, coating AgNPs with gold provides a range of opportunities to engineer nanostructures beneficial for applications, such as SERS and SPR sensing. [23,24]

Herein we demonstrate that designed thin-frame gold plating on silver nanoparticles enable enhanced SPR detection through morphological transformations. This straightforward plating procedure improves SPR sensitivity compared to AgNPs and uniformly gold-plated Au@AgNPs (gold at silver). For instance, 10^{-8} M of ampicillin, cysteine and bromide can be readily detected. As a result, the developed nanostructures offer a promising platform for sensitive plasmonic detection.

Gold coating or plating onto AgNPs is generally performed to enhance chemical stability.[21,22] At the same time, placing a more noble metal, gold, on a surface of a less electronegative metal, silver, can cause faster dissolution of a more reactive metal if only partial coating is produced. We reasoned that this scenario may be advantageous for enhanced sensing since functional groups that bind strongly to metals can also assist in metal dissolution. Previously, we demonstrated gold deposition predominantly on the edges of silver decahedra (AgDeNPs) to yield frame morphologies.[15] Consequently, we explored how to engineer plating with the smallest amount of gold that would be strong enough at the edges to reinforce the structural integrity and to preserve the nanoparticle shape. Such coating would ideally support nanoparticle cavitation or stellation without much rounding or shrinking and thus attain larger LSPR shifts to larger wavelengths (red shifts) that are characteristic of the formation of cavities or shells. We named such morphology tf-Au@AgNPs, denoting thick frames or thin fragile plating. The straightforward set of conditions to attain this morphology was realized through fast addition of an appropriately diluted gold precursor (tetrachloroauric acid) to a new generation of AgDeNPs[25,26] stabilized with poly (styrene sulfonate), PSS[27] (see Experimental in ESI).

[a] *Chemistry Department, Wilfrid Laurier University, 75 University Ave. W, Waterloo, Ontario, N2L 3C5, Canada. E-mail: vkitaev@wlu.ca*

† Electronic supplementary information (ESI) available: Experimental, additional UV-vis spectra and electron microscopy images. See DOI:10.1039/x0xx00000x

The results on tf-Au@AgNP formation are summarized in Fig. 1 and Fig. S1, ESI†. Continuous and smooth gold coating is produced with up to 4 mol. % of gold relative to silver in AgDeNPs (Fig. 1a-d). Starting from 4-5 mol. %, enhanced gold deposition around edges can be noticed (Fig. S2, ESI†). With even higher percentage of gold in tf-Au@AgNPs (>6 mol. %), dissolution of silver and formation of shell-like morphologies becomes apparent (Fig. 1e).

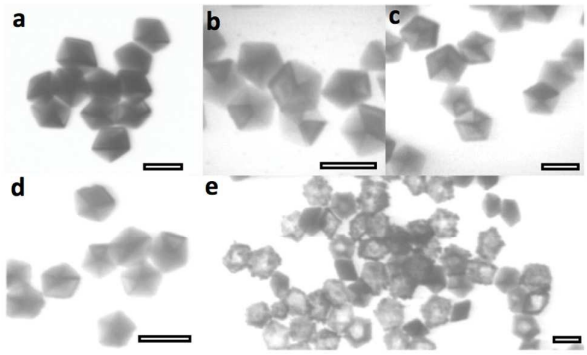

Fig. 1 Images of **a)** precursor AgDeNPs and **b)-e)** tf-Au@AgNPs with varying mol. % of gold plating relative to silver present in AgDeNPs: **b)** 0.25%, **c)** 1%, **d)** 4% and **e)** 8%. All scale bars are 50 nm.

Noteworthy, even 0.5 mol. Au % plating in tf-Au@AgNPs is sufficient to reinforce the edges and preserve the structural integrity of tf-Au@AgNPs upon silver etching. This leads to cavitation rather than uniform rounding and enables characteristic LSPR red shifts (Figs. 2 and 3). UV-vis graphs showing two independent series of formation of tf-Au@AgNPs with different mol. % of Au (Fig. S2, ESI†) support these findings: the LSPR peaks are well-defined for 0.5% and 1%, noticeably broader for 4-6%, and very broad for >8 mol. %. As well, the reproducibility of tf-Au@AgNP preparation is established.

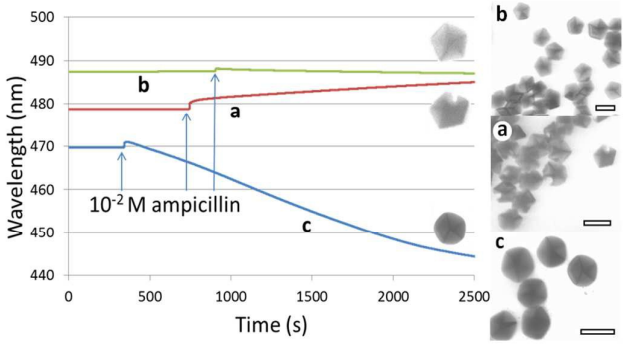

Fig. 2 Surface plasmon resonance (SPR) response curves and corresponding TEM images after addition of 10^{-2} M ampicillin to **a)** tf-Au@AgNPs with 1 mol. % Au, **b)** u-Au@AgNPs with 20 mol. % Au and **c)** unmodified AgDeNPs. Injection of analyte is indicated by the arrows. All scale bars are 50 nm.

Fig. 2 provides a comparison of characteristic SPR responses for unmodified AgNPs, uniformly plated AgNPs (u-Au@AgNPs) and tf-Au@AgNPs upon exposure to ampicillin. Ampicillin binds strongly to silver and gold NPs[28] by thioester and amine groups and first causes LSPR changes (red shift) due to chemisorption.[29,30] Furthermore, strong ampicillin binding to silver enhances its partial dissolution from tf-Au@AgNPs(Fig. 2a). Thiols complex Ag^+ and Au^+ strongly as soft metals. Binding of silver ions reduces their concentration and shifts the red-ox equilibrium towards dissolution of the metal, as expressed by the Nernst equation.

In unmodified AgNPs, partial dissolution results in rounding, as can be seen in electron microscopy images (Fig. 2c) and a corresponding decrease (blue shift) in LSPR peak values.

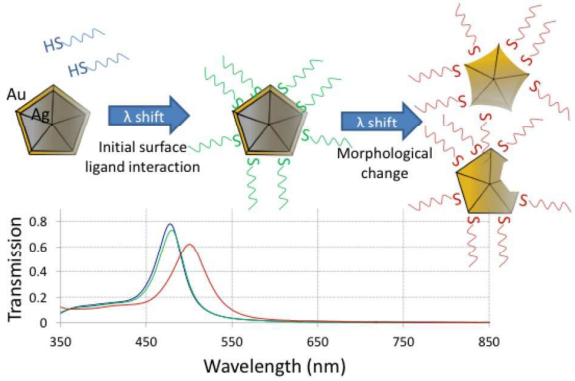

Fig. 3 Schematic illustration of morphologically-enhanced sensing by tf-Au@AgNPs upon addition of silver-binding analytes. Two parts of LSPR response originate first from ligand chemisorption and then morphological transformation of tf-Au@AgNPs by cavitation and stellation.

Uniformly plated u-Au@AgNPs behave similar to gold NPs and experience minimal LSPR changes (Fig. 2b), with the exception of small changes due to chemisorption, which are less resolvable in the scale of Fig. 2. The stability of u-Au@AgNPs SPR signal exposed to 10^{-2} M ampicillin is further demonstrated in Fig. S3, ESI†. In contrast to u-Au@AgNPs, tf-Au@AgNPs exhibit a larger increase in LSPR peak wavelength (Fig. 2a). As illustrated in EM images (Fig. 2a), the origin of this shift is the partial removal of interior silver leading to the appearance of characteristic "bitten" or cavitated structures[31] (Fig. 3). For the SPR sensing, the blue LSPR shift experienced by AgNPs upon rounding is opposite in direction to the LSPR increase due to chemisorption, and thus masks or deteriorates the SPR signal upon adsorption. In contrast, the red LSPR shift associated with tf-Au@AgNP shellation enhances the chemisorption response, as can be seen from the comparison with u-Au@AgNPs.

Fig. 3 presents a schematic of morphological changes of tf-Au@AgNPs upon ampicillin exposure together with the corresponding UV-vis spectra elaborating on the SPR changes. First, within 100-200 seconds, chemisorption of thiols (or amines) takes place with the corresponding relatively small increase in SPR signal of 0.3 to 2 nm (depending on analyte concentration). Subsequently, at longer exposure times, more pronounced SPR changes (>10 nm) take place as a result of the partial removal of silver and formation of "bitten" or cavitated structures. These morphological changes are instrumental for the enhancement of SPR sensing. With the slope of the LSPR increase of 0.0043 nm/s due to shellation (see data of Fig. S5), the signal enhancement can be very appreciable (0.5-1.3 nm during 2-5 minute probing times typical for SPR

measurements). If longer measurement times are feasible, even stronger signal enhancement can be realized.

The long-term SPR response of tf-Au@AgNPs with varying mol. % of gold is compared in Fig. S4, ESI† to assess the best SPR enhancement range. The strongest SPR response is observed for 1%, which manifests in a higher slope and a correspondingly higher sensitivity (Fig. S4 and Fig. S5, ESI†). This observation can be attributed to the gold presence enhancing silver dissolution of non-uniformly plated nanoparticles. For lower % of gold, e.g. 0.5%, the SPR response diminishes since gold frames of the cavitated structures are weaker and may become partially dissolved or rounded (rounding causes opposing blue shifts in the SPR signal as a result of decreasing NP dimensions). For the larger % of gold, e.g. 5 and 6 mol. %, an initial dip in SPR peak values is observed which can be linked to partial degradation of already pitted Au@AgNPs (as seen in Fig. 1e). In addition to cavitated morphologies (Fig. 2a and Fig. S6, ESI†), stellated structures were also observed after exposure of tf-Au@AgNPs with a relatively low gold content of 0.5-1.5 mol. % to strongly binding analytes, such as ampicillin (Fig. S7, ESI†). Stellation arises upon partial dissolution of tf-Au@AgNPs, when the gold-enriched surface layer is preferentially preserved, particularly at the vertices, being more resistant to etching.

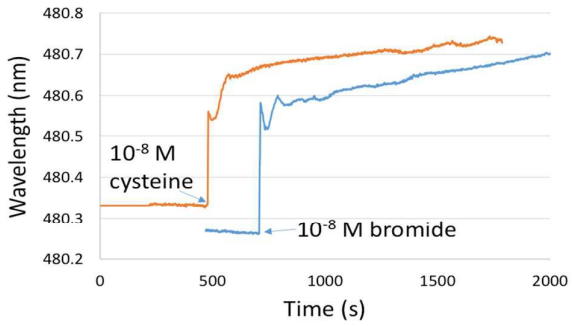

Fig. 4 SPR response curve of tf-Au@AgNPs with 1 mol. % upon exposure to 10^{-8} M cysteine and bromide. Injection of analytes are indicated by the arrows. The curves are offset in time for clarity of presentation.

tf-Au@AgNPs with 1 mol. % of gold were selected for prototype SPR sensing experiments due to their highest sensitivity (Fig. 4 and Fig. S8, ESI†). The SPR response can readily resolve addition of 10^{-8} M of cysteine and bromide as analytes chemisorbing on tf-Au@AgNPs. Additional information on SPR response to iodide and ampicillin is presented in Fig. S8 in ESI†. Histidine, as a strongly binding amine, could also be detected at 10^{-8} M. The well-defined SPR response is clearly enhanced by morphological changes manifesting themselves in an upward slope of the signal. The background of the signal of an undisturbed cell is ca. 0.02 nm (Fig. S9, ESI†). At the same time, the cell disturbance upon analyte addition can be as high as 0.1 nm (Fig. S8, ESI†) which currently limits reliable detection of cysteine, ampicillin and bromide to ca. 10^{-8} M at S/N=3. Iodide, being the largest most polarizable anion, can be detected at lower concentrations of ca. 5×10^{-9} M, in line with what was previously reported for stellated AuNPs.[32]

We have performed comparative tests with chloride that is a main component of biological media and is known to interfere with the SPR response of AgNPs. Surprisingly, tf-Au@AgNPs are stable to 0.1 M chloride for the time of SPR probing, while AgNPs etch rapidly (Fig. S10, ESI†). Chloride physisorption is clearly observable in the SPR response (Fig. S10, ESI†). Physisorption of chloride does not interfere with detection of 10^{-8} M cysteine (Fig. S11A, ESI†) since thiols bind more strongly than halides to AgNPs. Similarly, the SPR response to 10^{-8} M cysteine can be reliably detected in presence of phosphate-buffered saline, a commonly used buffer solution in biological research (Fig. S11B, ESI†). Furthermore, a sequential SPR response to iodide and cysteine can be observed at concentrations as low as 10^{-9} M and 10^{-8} M, respectively (Fig. S12, ESI†) Future work will involve more systematic studies of sensing biologically relevant analytes and further development of gold-plated AgNPs for sensitive SPR detection.

In conclusion, we have described the preparation and functionality of tf-Au@AgNPs, gold-plated silver morphologies, advantageous for SPR sensing compared to uniformly plated Au@AgNPs and non-modified AgNPs. The developed and enhanced SPR sensing platform, which amplifies the response to analytes through morphological changes, is herein reported for the first time. These morphological transformations due to partial silver etching enable sensitive and reliable detection of 10^{-8} M of ampicillin, histidine, cysteine and bromide.

The authors thank NSERC (Discovery grant and graduate scholarships) and ACS PRF for funding. Centre for Nanostructure Imaging, University of Toronto, is acknowledged for access to imaging facilities, and Ilya Gourevich and Neil Coombs for their invaluable support with the electron microscopy.

Notes and references

1 J. Langer, S. M. Novikov and L. M. Liz-Marzán, *Nanotechnology* 2015, **26**, 322001.
2 J. Sun, Y. Xianyu and X. Jiang, *Chem. Soc. Rev*. 2016, **43**, 6239–6253.
3 Q. Chen, Y. Jia, S. Xie and Z. Xie, *Chem. Soc. Rev.* 2016, DOI: 10.1039/c6cs00039h
4 H. Lui, F. Nosheen and X. Wang, *Chem. Soc. Rev.* 2015, **44**, 3056–3078.
5 D. A. Tomalia and S. N. Khanna, *Chem. Rev.* 2016, **116**, 2705–2774.
6 X. Xia, Y. Wang, A. Ruditskiy and Y. Xia, *Adv. Mater.* 2013, **25**, 6313–6333.
7 N. S. Abadeer and C. J. Murphy, *J. Phys. Chem. C* 2016, **20**, 4691–4716.
8 N. Cathcart and V. Kitaev, *Nanoscale*, 2012, **4**, 6981–6989.
9 M. Jahn, S. Patze, I. J. Hidi et. al. *Analyst* 2016, **141**, 756–793.
10 J. Li, T. Zhao, T. Chen, Y. Liu, C. N. Ong and J. Xie, *Nanoscale*, 2015, **7**, 7502–7519.
11 Z. Yuan, C.-C. Hu, H.-T. Chang and C. Lu, *Analyst* 2016, **141**, 1611–1626.
12 K.-S. Lee and M. A. El-Sayed *J. Phys. Chem. B*, 2006, **110**, 19220–19225.
13 K. L. Gōeken, V. Subramaniam and R. Gill, *Phys. Chem. Chem. Phys.* 2015, **17**, 422–427.

14 J. Prasad, I. Zins, R. Branscheild, J. Becker, A. H. R. Koch, G. Fytas, U. Kolb and C. Sönnichsen, *J. Phys. Chem. C.* 2015, **119**, 5577–5582.
15 M. McEachran, D. Keogh, B. Pietrobon, N. Cathcart, I. Gourevich, N. Coombs and V. Kitaev, *J. Am. Chem. Soc.,* 2011, **133**, 8066–8069.
16 C. Gao, Z. Lu, Y. Liu, Q. Zhang, M. Chi, Q. Cheng and Y. Yin, *Angew. Chem. Int. Ed.,* 2012, **51**, 1–6.
17 Y. Y. Ma, W. Y. Li, E. C. Cho, Z. Y. Li, T. K. Yu, J. Zeng, Z.X. Xie and Y. Xia, *ACS Nano*, 2010, **4**, 6725–6734.
18 J. D. Padmos, M. L. Personick, Q. Tang, P. N. Duchesne, D.-E. Jiang, C. A. Mirkin and P. Zhang, *Nature Commun.* 2015, **6**, 7664.
19 K. Jia, M. Y. Khaywah, Y. Li, J. L. Bijeon, P. M. Adam, R. Deturche, B. Guelorget, M. Francois, G. Louarn and R. E. Ionescu, *ACS Appl. Mater. Interfaces* 2014, **6**, 219–227.
20 T. Lou, L. Chen, Z. Chen, Y. Wang, L. Chen and J. Li, *ACS Appl. Mater. Interfaces* 2011, **3**, 4215–4220.
21 N. Murshid, I. Gourevich, N. Coombs and V. Kitaev, *Chem. Commun*., 2013, **49**, 11355–11357.
22 Y. Yang, J. Liu, Z.-W. Fuand D. Qin, *J. Am. Chem. Soc.,* 2014, **136**, 8153–8156.
23 J. Zhang, S. A. Winget, Y. Wu, D. Su, X. Sun, Z.-X., Xie and D. Qin, *ACS Nano*, 2016, **10,** 2607–2616.
24 P. Dong, Y. Lin, J. Deng and J. Di, *ACS Appl. Mater. Interfaces* 2013, **5**, 2392–2399.
25 B. Pietrobon and V. Kitaev, *Chem. Mater.,* 2008, **20**, 5186–5190.
26 N. Murshid, D. Keogh, V. Kitaev, *Part. Part. Syst. Charact.* 2013*,* **31**, 178–189.
27 N. Murshid, V. Kitaev, *Chem. Commun*., 2014, **50**, 1247–1249. .
28 N. Tarrat, M. Benoit, M. Giraud, A. Ponchet and M. J. Casanove, *Nanoscale*, 2015, **7**, 14515–14524.
29 A. P. Gondikas, A. Morris, B.C. Reinsch, G.V. Lowry and H. Hsu-Kim, *Environ Sci Technol.,* 2012, **46**, 7037–7035.
30 J. M. Zook, S. E. Long, D. Cleveland, C. L. A. Geronimo and R. I. MacCuspie, *Anal. Bioanal. Chem.*, 2011, **401**, 1993–2002.
31 Y. Sun, B. Mayers and Y Xia, *Adv. Mater*. 2003, **15**, 641–646.
32 R. Keunen, D. Macoretta, N. Cathcart and V. Kitaev, Nanoscale, 2016, **8**, 2575–2583.

TOC image

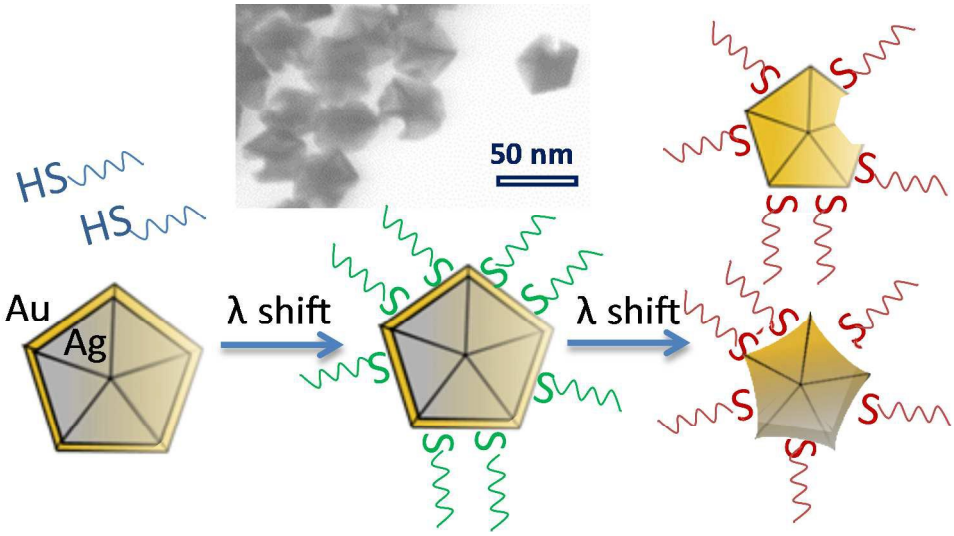

TOC text:

Morphological changes of gold-plated silver nanoparticles enhance SPR sensing